

Shallow crust structure of the Büyük Menderes graben through an analysis of gravity data

F. Figen ALTINOĞLU^{1*}, Murat SARI², Ali AYDIN¹

¹Department of Geophysical Engineering, Faculty of Engineering, Pamukkale University, Denizli, Turkey

²Department of Mathematics, Faculty of Arts and Science, Yıldız Technical University, İstanbul, Turkey

Received: 07.12.2017 • Accepted/Published Online: 17.07.2018 • Final Version: 30.11.2018

Abstract: The Büyük Menderes is one of the most important geostructural features of highly seismically active western Anatolia, Turkey. This article aims to analyze the geological features and the shallow crust structure of the Büyük Menderes graben. To achieve this, six different edge detection filters and a 3D inversion method were applied to the Bouguer gravity data to detect new lineaments and shallow crust topographies. A renewed fault map of the Büyük Menderes graben is the significant contribution of the present study. New lineaments were detected in the western, southeastern, and northern parts of the region, where intense seismicity was observed. The basement, the upper-lower crust undulation, and their relations were analyzed in detail. The maximum sediment thickness was defined as 4.1 km. The subsurface depths are increasing in N-S and W-E directions. The new determined lineaments may be a topic of future research to warrant attention.

Key words: Basement undulation, upper-lower crust undulation, Büyük Menderes, lineament, shallow basement

1. Introduction

Western Anatolia is a tectonically complex, seismically active, lithospheric extension and thinning region. The mainly E-W trending Büyük Menderes and Gediz grabens are the most specific structures of the region. The active tectonics in western Anatolia are controlled by the synergetic movement of the Eurasian, African, and Arabian plates (Figure 1). The age and origin of this extension mechanism are debatable and have been explained by the following different models: (a) the tectonic escape model (Dewey and Şengör, 1979; Şengör et al., 1985); (b) the back-arc spreading model (McKenzie, 1972; Le Pichon and Angelier, 1979); (c) the orogenic collapse model (Seyitoğlu et al., 1992; Seyitoğlu and Scott, 1996); (d) the episodic model (Koçyiğit et al., 1999; Bozkurt and Sözbilir, 2004, 2006).

Mainly the E-W and the NE-SW trending Neogene to Quaternary continental basins occurred in the region under a N-S directional extension regime (Şengör et al., 1985; Yılmaz et al., 2000). The Gediz and Büyük Menderes grabens are characterized by Miocene detachment faulting and core-complex formation, and high angle normal faulting controlled the Plio-Quaternary graben floor fillings with 140 km in length and 2.5–14 km in width, localized to the north and the south by the Menderes Massif metamorphic complex (Yılmaz et al., 2000; Sözbilir,

2001; Bozkurt and Sözbilir, 2004, 2006; Çiftçi and Bozkurt, 2009).

Many geophysical studies carried out by various authors (Sarı and Şalk, 2002, 2006; Göktürkler et al., 2003; Pamukçu and Yurdakul, 2008; Işık and Şenel, 2009; Çiftçi et al., 2011; Akay et al., 2013; Altinoğlu and Aydın, 2015; Bayrak et al., 2017; Çubuk-Sabancı et al., 2017) were conducted on western Anatolia, including the Büyük Menderes graben region. Many of them revealed the 2D or 3D basement depths (Sarı and Şalk, 2002, 2006; Işık and Şenel, 2009), and Göktürkler et al. (2003) revealed the 2D crust model for a profile including important grabens of western Anatolia, as well as the Büyük Menderes graben. However, to the best of our knowledge, to determine the detailed structural features, mapping in the whole graben has not been studied in detail yet. Differently from previous studies, we have estimated both the basement and upper/lower crust boundaries and explored a new lineament map of the Büyük Menderes graben area by using gravity data. Determination of tectonic structures of a region is of importance since it provides information for researchers on seismicity, industrial material searches, and geothermal potentiality of that region. In this respect, this study aims to produce updated structural features of the Büyük Menderes basin (Figure 1) and its shallow crust interface topographies. Thus, some new lineaments in the

* Correspondence: faltinoglu@pau.edu.tr

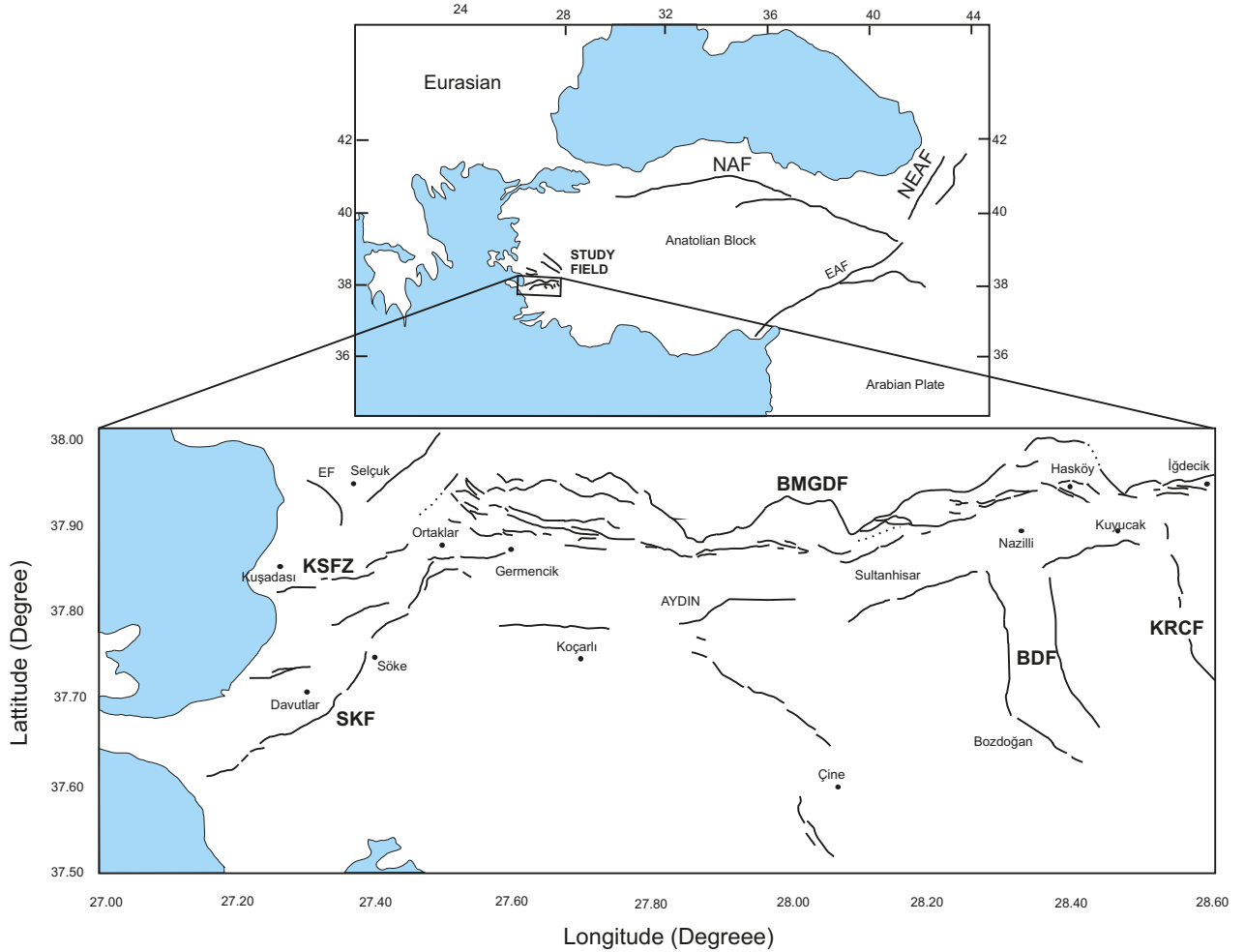


Figure 1. Simplified tectonic map of Anatolian region and study area. NAF: North Anatolian Fault, EAF: East Anatolian Fault, NEAF: North East Anatolian Fault, BMGDF: Büyük Menderes Graben Detachment Fault, EF: Efes Fault, KSFZ: Kuşadası Fault Zone, SKF: Söke Fault, BDF: Bozdoğan Fault, KRCF: Karacasu Fault, CF: Çine Fault.

Büyük Menderes graben were discovered by using edge detection methods. Some of these methods were also used by the authors to investigate the Denizli graben, located at the westward continuation of the Büyük Menderes graben in western Anatolia (Altinoğlu et al., 2015).

2. Gravity surveys

Gravity anomalies have been used as a powerful tool for geological mapping (Nabighian et al., 2005; Gout et al., 2010; Uieda and Barbosa, 2012; Guo et al., 2014; Wang et al., 2014; Chen et al., 2015; Ali et al., 2017; Wang, 2017). To define the linear features and the crustal structure of the basin, the Bouguer gravity anomaly data provided by a joint study of the General Directorate of Mineral Research and Exploration of Turkey (MTA) and the Turkish Petroleum Corporation (TPAO) were used. The data were taken at station spacing of 250–500 m with accuracy of 0.1 mGal and then the data were gridded over areas of 1 km².

The contour interval of the map shown in Figure 2 is 2 mGal. The gravity anomaly values range from –35 to 75 mGal with an increasing regional tendency from the east to the west and the minimum values emerged as a result of the crust thinning and thickening of sedimentary basins. Sedimentary basins are generally related to low gravity values based on the low-density sediments in them (Sarı and Şalk, 2002). Positive gravity anomalies monitored at the west of the graben are interpreted as a positive anomaly belt attendance of a concave side of island arc related to the uplifted mantle (Rabinowitz and Ryan, 1970; Özelçi 1973).

To obtain the lineament map of the study area, some edge detection filters were applied to Bouguer gravity anomaly data by using the computer code given by Arısoy and Dikmen (2011). New detailed basement and upper-lower crust boundaries were produced with the use of a computer code presented by Gómez-Ortiz and Agarwal (2005). To present the seismic activity of the faults or to

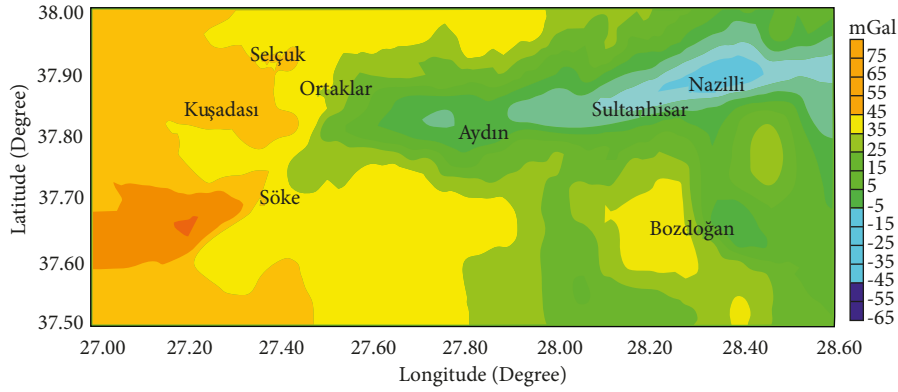


Figure 2. Bouguer gravity anomaly map of the study area (contour interval is 10 mGal).

see if the probable detected new lineament was seismically active, the epicentral distribution of the earthquakes that occurred in the region was produced in terms of the data from 2000 to 2017 (<http://www.koeri.boun.edu.tr/sismo/zeqdb/>).

3. Methods

The power spectrum method developed by Spector and Grant (1970), which also utilizes 2D Fourier transform of potential field data, was used to detect the average depths of the crust layers.

Many studies in the literature (Hahn et al., 1976; Connard et al., 1983; Bosum et al., 1989; Garcia-Abdeslem and Ness, 1994) used the power spectrum method applied in the current study. Figure 3 clearly reveals that three distinct layers were discovered in the study area.

The Parker–Oldenburg algorithm, based on the relationship between the Fourier transform of the gravity data and the sum of the interface topography's transform (Parker, 1972; Oldenburg, 1974), was used to enhance the three-dimensional interface topography. The Fourier transform given in Eq. (1) is used to calculate the gravity anomaly of an uneven homogeneous layer.

$$F[z_1(x)] = -\frac{F[\Delta g(x)]e^{k|z_0}}{2\pi Gg} - \sum_{n=2}^{\infty} \frac{|k|^{n-1}}{n!} F[z_1^n(x)] \quad (1)$$

Here, $f[\Delta g(x)]$, G , k , g , $z_1(x)$, and z_0 indicate the Fourier transform of the gravity anomaly, gravitational constant, wave number, density of the layer, depth to interface, and average depth of horizontal interface, respectively. In the equation, density interface topography is calculated from $\Delta g(x)$ and z_0 in the iteration process. In the iteration algorithm, either $z_1=0$ or an appropriate value is designated for the right part of the formula. The first estimation of the topographical conditions was enhanced by inverse Fourier transform. This topography parameter is considered to determine the right-hand side of the formula. The result obtained from the first prediction

is used to reach the second topography approach. The iteration process continues until the convergence criterion is reached. To investigate the features of the study region, some edge detection techniques were also considered here more closely.

Edge detection of a source body is a useful tool in the interpretation of gravity anomalies, which were widely used in exploration technologies for mineral resources (Mickus, 2008; Chen et al., 2015), geothermal exploration (Saibi et al., 2006; Ali et al., 2015; Nishijima and Naritomi, 2015), and mapping geological boundaries such as faults, buried faults, and lineaments (Rapolla et al., 2002; Ardestani, 2005; Ardestani and Motavalli, 2007; Kumar et al., 2009; Oruç, 2010; Cheyney et al., 2011; Naouali et al., 2011; Ma and Li, 2012; Ekinici et al., 2013; Hoseini et al., 2013; Alvandi and Rasoul, 2014; Wang et al., 2015; Zuo and Hu, 2015; Alvandi and Babaei, 2017; Elmas et al., 2018).

3.1. Horizontal gradient magnitude

The horizontal gradient magnitude (HGM) method is a useful tool in determining the surface or buried faults (Cordell and Grauch, 1985; Hornby et al., 1999; Phillips, 2000; Rapolla et al., 2002; Lyngsie et al., 2006; Saibi et al., 2006). HGM was first given by Cordell and Grauch (1985):

$$HG = \sqrt{\left(\frac{\partial g}{\partial x}\right)^2 + \left(\frac{\partial g}{\partial y}\right)^2} \quad (2)$$

Here, $\frac{\partial g}{\partial x}$ and $\frac{\partial g}{\partial y}$ are the first-order derivatives of the gravity field in the orthogonal directions.

HGM is very effective in highlighting both shallow and deep geological bodies. The maximum values of the HGM are located at abrupt changes of density and indicate the source edges (Cordell, 1979; Cordell and Grauch, 1985, Cooper and Cowan, 2004).

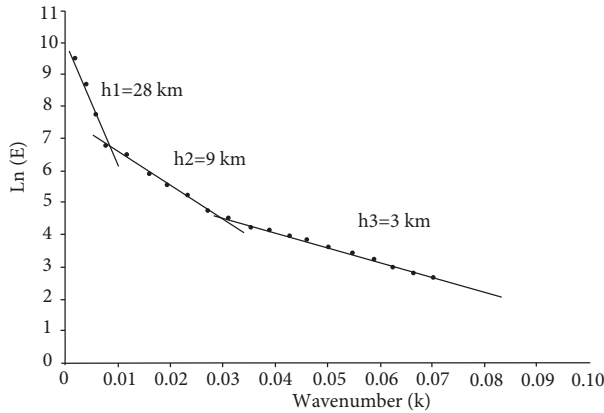


Figure 3. The power spectrum of the Bouguer gravity anomaly of the study area.

3.2. Analytic signal

The analytic signal tool was first applied to potential field data by Nabighian (1972). The approach is utilized to define the magnitude of the total gradient of the magnetic anomaly and mathematically given as:

$$A(x, y) = \sqrt{\left(\frac{\partial f}{\partial x}\right)^2 + \left(\frac{\partial f}{\partial y}\right)^2 + \left(\frac{\partial f}{\partial z}\right)^2} \tag{3}$$

Here, f is the first vertical derivative ($\partial g/\partial z$) of the gravity field. Similar to the horizontal gradient, it generates maximum values over source edges (Nabighian, 1972, 1984; Roest et al., 1992).

3.3. Tilt angle

The tilt angle technique, first proposed by Miller and Singh (1994), was applied to the gravity data. The following ratio constitutes the zero values of the tilt angle map, which show the boundary of the bodies. The equation was given by Miller and Singh (1994) as follows:

$$\phi = \tan^{-1} \left[\frac{\frac{\partial f}{\partial z}}{\sqrt{\left[\left(\frac{\partial f}{\partial x}\right)^2 + \left(\frac{\partial f}{\partial y}\right)^2\right]}} \right] \tag{4}$$

Here, ϕ indicates the tilt angle parameter.

The tilt angle is positive over a source and zero values reflect the source edges (Miller and Singh, 1994). This method is useful in enhancing edges of anomalies for both shallow and deep sources. The tilt angle of the first vertical gradient of the gravity data provides a new tilt angle. It was first used by Oruç (2010) and is given as:

$$\phi = \tan^{-1} \left[\frac{\frac{\partial^2 g}{\partial z^2}}{\sqrt{\left[\left(\frac{\partial g}{\partial x \partial z}\right)^2 + \left(\frac{\partial g}{\partial y \partial z}\right)^2\right]}} \right] \tag{5}$$

The tilt angle is thus obtained from the second vertical gradient ($\partial^2 g/\partial z^2$) and the HGM. Oruç (2010) remarked that the practical utility of the technique is demonstrated to improve the gravity resolution and emphasized the effects of the geological boundaries for the structural framework.

3.4. Tilt derivative

First, Verduzco et al. (2004) calculated the HGM of the tilt angle (TA), given by:

$$TD = \sqrt{\left(\frac{\partial TA}{\partial x}\right)^2 + \left(\frac{\partial TA}{\partial y}\right)^2} \tag{6}$$

The maximum values of the total horizontal derivative of the tilt angle represent the source body edges (Cooper and Cowan, 2006).

3.5. Theta map

The theta map is a combination of the HGM and the analytic signal, described by Wijns et al. (2005) to use for edge detection. It is given as:

$$\cos(\theta) = \frac{\sqrt{\left(\frac{\partial g}{\partial x}\right)^2 + \left(\frac{\partial g}{\partial y}\right)^2}}{|A|} \tag{7}$$

Here, |A| is the analytic signal amplitude. The maximum values are observed within the structure even as minimum values are seen along the source body edges in the theta map.

3.6. Hyperbolic tilt angle

The hyperbolic tangent (HTA) function was expressed by Cooper and Cowan (2006) as:

$$HTA = \tanh^{-1} \frac{\frac{\partial g}{\partial z}}{\sqrt{\left[\left(\frac{\partial g}{\partial x}\right)^2 + \left(\frac{\partial g}{\partial y}\right)^2\right]}} \tag{8}$$

The maximum value of the HTA generates the location of the source body edges.

4. Results and discussion

By using the Bouguer gravity anomaly data, the linear features and the 3D subsurface undulation of the Büyük Menderes graben and surroundings were carefully studied in the present work. The Büyük Menderes graben has E-W trending negative gravity anomalies. The gravity anomaly values of western Anatolia get higher from the east to the west (Sarı and Şalk 2002). It is understood, as pointed out

by Sarı and Şalk (2002), that the decreasing of the anomaly values from west to east is related to low density and the crust thinning in the western Anatolian region.

Three subsurface levels have been determined as 3 km, 9 km, and 28 km by the slopes of the power spectrum-wave number graph of the gravity data as clearly seen in Figure 3, representing the sediment thickness, the upper-lower crust boundary, and the Moho depth, respectively.

To analyze the shallow crust structure of graben area, the sediment and the upper-lower crust boundary topographies were computed using a computer code produced in MATLAB based on the Parker–Oldenburg algorithm (Parker, 1972; Oldenburg, 1974).

To produce the sediment topography, the initial depth in the iteration process is taken to be 3 km. The average density contrast is considered to be 0.3 g/cm^3 between Neogene sediments until the crystalline basement level ($\sim 2.4 \text{ g/cm}^3$) and metamorphic complex ($\sim 2.7 \text{ g/cm}^3$). The

obtained sediment topography map is provided in Figure 4.

The maximum depth of the sedimentary basin is observed to be 4.1 km between Sultanhisar and Nazilli and the sediment thickness is seen to be decreasing from east to west and from south to north. The maximum sediment thickness of the Büyük graben was determined as 1.5–2 km by Sarı and Şalk (2002), 2.5 km by Göktürkler et al. (2003), and 3.9 km by Işık and Şenel (2009) in the literature. The sediment thickness was determined as 1.5 km at Aydın by Cohen et al. (1995), and between Aydın and Sultanhisar as 2.0–2.2 km by Işık (1997) and 2.0 km by Sarı and Şalk (2006). The sediment thickness between Sultanhisar and Nazilli was determined as 2.2–2.3 km by Işık (1997) and 2.5 km by Şenel (1997). The differences in thickness are believed to stem from the consideration of different density contrast values. The graben structure in the region deepens from north to south and from west to east as mentioned in the work of Işık and Şenel (2009).

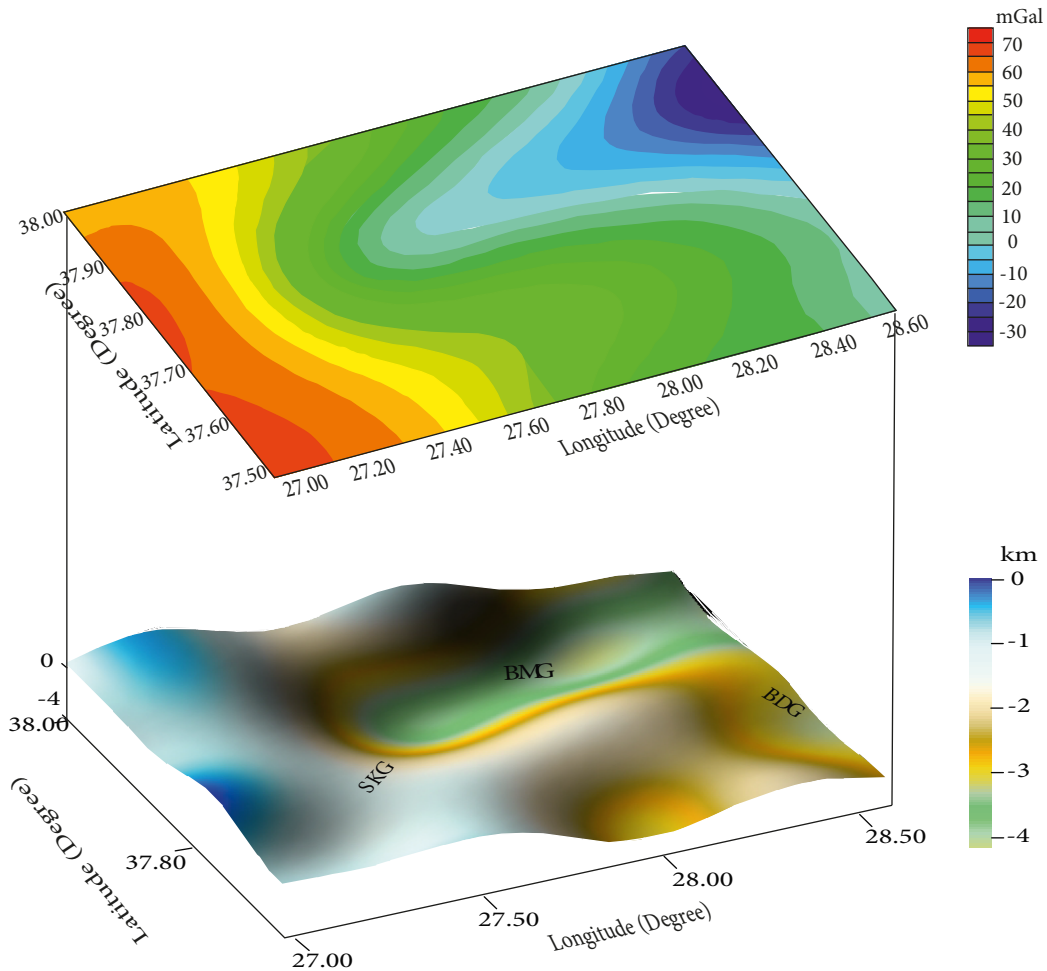


Figure 4. The basement undulation map of the study field derived from inversion of the Bouguer gravity anomalies of the study area by using the Parker–Oldenburg’s algorithm. BMG, SKG, BDG: Büyük Menderes Graben, Söke Graben, Bozdoğan graben, respectively.

To produce the upper-lower crust boundary topography, the initial depth in the iteration process is taken to be 9 km. The average density contrast is considered to be 0.4 g/cm^3 between average crust density ($\sim 2.7 \text{ g/cm}^3$) and the material below the assumed flexed elastic plate ($\sim 3.1 \text{ g/cm}^3$). The obtained upper-lower crust boundary topography ranges from 4.50 to 12.50 km and shallows from east to west, as seen in Figure 5. These results reveal that the anomalies of the study area are compatible with the upper-lower crust topography. It is noticeable that the upper-lower crust boundary takes the maximum depth of 12.50 km in Nazilli, where the gravity anomaly values are about -35 mGal . The upper-lower crust boundary ranges from 8.50 km to 11.50 km between Ortaklar and Sultanhisar and from 11.50 km to 12.50 km at the Sultanhisar-Nazilli line. The depths are

seen to be 10–11 km and 7–9 km at the Bozdoğan graben and at the Söke basin, respectively. It is important to point out that a new basin structure was detected in the N-S direction in the south of the Büyük Menderes graben (see Figure 5). It can be readily seen from both Figure 4 and Figure 5 that the basement topographies improved under the same tectonism with the lineaments bounding the Büyük Menderes graben. Both basement topographies are seen to have the same behavior that shows minimum and maximum values in the same area. Our observations are supported by the work of Çiğçi et al. (2011).

To discover the linear features of the study area, the horizontal gradient, analytic signal, first vertical gradient, tilt angle, tilt angle of vertical gradient, tilt derivative, theta map, and hyperbolic tilt angle edge detection methods

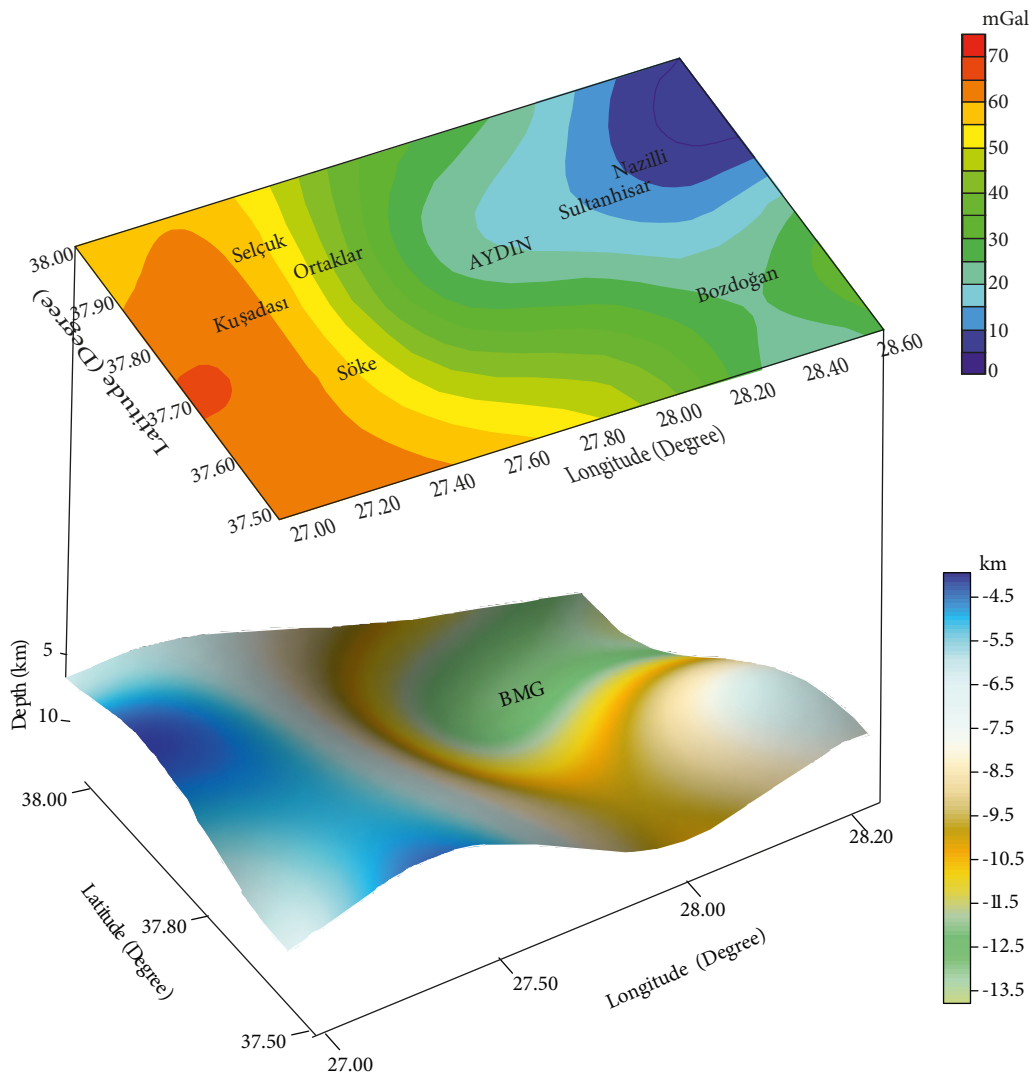


Figure 5. The upper-lower crust boundary's topography map of the study region derived from inversion of the Bouguer gravity anomalies using the Parker–Oldenburg's algorithm. BMG: Büyük Menderes graben.

were applied to the Bouguer gravity anomaly data. In general, faults are expected to be situated at or near the steepest gradient of the anomaly. As pointed out by Gout et al. (2010), this characteristic is particularly helpful in areas where the fault zone is concealed by younger sedimentary deposits. The maximum value of the HGM and analytic signal indicate the source edge, and maximum values indicate the boundary faults of the graben mainly on the E-W and the SW-NE trends (see Figures 6a and 6b). The first vertical gradient map is given in Figure 6c. The zero values of the tilt angle map show the boundary of the source edge, so in the tilt angle map zero values are pointed out by red lines in Figure 6d. The zero values of the tilt angle of the vertical gradient map show the boundary of the source edge, and zero values of the tilt angle of the vertical gradient are pointed out by red lines in Figure 6e.

The resolution of this map is good. The maximum values are monitored within the source in the theta map given in Figure 6f. Its maximum values are in agreement with the horizontal gradient and analytic signal maximum values, but it is more sensitive to detecting probable new shallow faults than deep boundary faults. The tilt derivative produces maximum values vertically above the edges of source bodies, so it is easy to delineate vertical faults with its maximum as seen in Figure 6g. The maximum value of the hyperbolic tilt angle points out the location of the source body edges. As seen in Figure 6h, the minimum values of the hyperbolic tilt angle show the boundary of the basin and the maximum values of the hyperbolic tilt angle give the faults.

The enhanced maps of the lineaments based on the edge detection methods are presented in Figures 6a–6h.

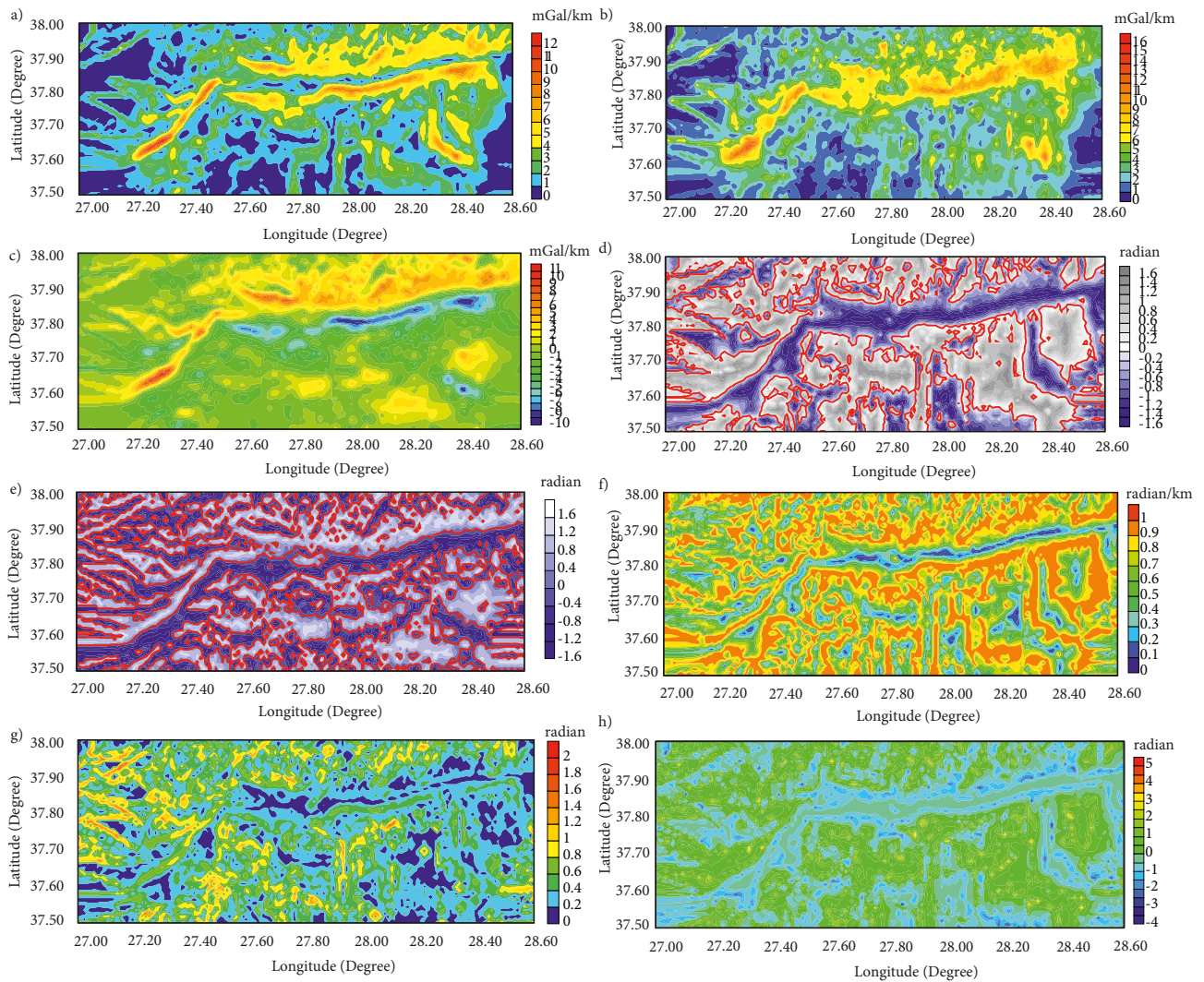


Figure 6. a) Horizontal gradient map. b) Analytic signal map. c) First vertical derivative map. d) Tilt angle map. e) Tilt angle map of first vertical derivative. f) Theta map. g) Tilt derivative map. h) Hyperbolic tilt angle map of the study field.

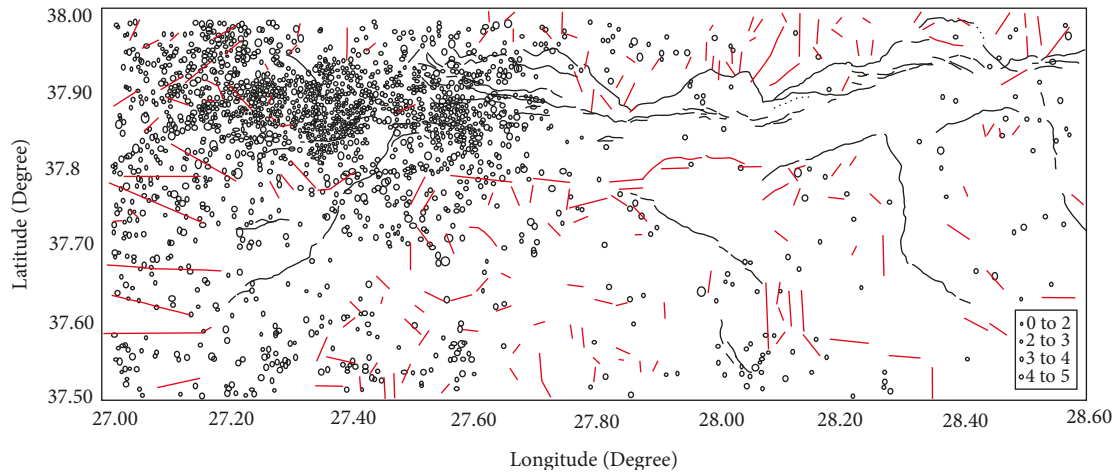


Figure 7. The epicentral distribution map of the earthquakes that occurred in the study area with the new fault. Faults in the study region are shown in black and newly detected lineaments are shown in red.

For comparison purposes, different methods were used to reach the results. The obtained results are seen to usually be in good agreement (see Figures 6a–6h). The lineaments that come out in the four methods are assumed to be lineaments in a general sense. The results show that almost all methods distinguished the E-W and NE-SW structural trends and all filters delineated edges of the graben successfully. The obtained lineaments are seen to be in agreement with the lineaments given by the MTA (Duman et al., 2011; Emre et al., 2011). Most of the lineaments identified are the boundary faults of the Büyük Menderes, Karacasu, and Bozdoğan grabens. Note that many newly discovered faults have been presented in the western, northern, and southern parts of the considered area.

The obtained structural map is consistent with many faults already recognized, and it highlights many new linear features. In order to underpin the current findings about the faults, the study region of interest was also interpreted with the aspect of earthquake activity. As seen from Figure 7, the region has high seismic activity; the western part of the area is the most active part and most of the earthquakes took place on the northern boundary of the Büyük Menderes graben.

In the study area, except for the main faults bounding the basins, many lineaments that were not previously discovered in the active fault map have been determined. High seismic activity has been observed in the areas where these new lineaments were identified.

In the basement undulation map, lineaments have been determined near the Selçuk, Nazilli, and Söke districts of the study, shaping the topography and extending to the bottom of the basement. The upper-lower crust undulation map in the basin of the south of the study area is noticeable. Thus, as seen in Figure 7, the newly determined lineaments

in the bottom topography extend to the depth of the base between Bozdoğan and Çine.

5. Conclusions and recommendations

The present study, carried out based on edge detection techniques and a 3D inversion approach to gravity data, has mainly produced the following conclusions:

1) The maximum depth of the sedimentary basin of the Büyük Menderes graben is observed to be 4 km. The sedimentary thickness is seen to be decreasing from east to west and from south to north. The thicknesses of the other basins in the study area, the Karacasu and Bozdoğan grabens, have been determined to be 2 km.

2) The obtained upper-lower crust boundary undulation is ranging from 4.50 to 12.50 km.

3) Both topographies, presented for the first time in the whole Büyük Menderes graben area, are seen to be correlated with each other. The depth level increases from east to west and from north to south in the region of interest.

4) As is the case in the literature, it is understood from our results that faults in the E-W direction of the Büyük Menderes graben separate horsts and grabens. It is concluded that the currently obtained topographies and the faults bounding the Büyük Menderes graben have been improved due to the same tectonic effect.

5) In terms of seismicity of the region, the newly determined sediment and upper-lower crust boundary topographies and the lineaments revealed that the basin is controlled by deep faults under the joint effect of the Cyprus Island Arc, Ölüdeniz Fault Zone, and Isparta Angle.

With this study, layer topographies of the Büyük Menderes were detected and the Büyük Menderes's

crust structure as well as basin geometry were revealed. The results obtained from the study provide valuable information for geologists to delineate the faults and other tectonic features.

In future studies, the focus may be on the newly detected faults and special interest may be given to seismological events.

References

- Akay T, Bilim F, Koşaroğlu S (2013). Investigation of the tectonic structures of Menderes massive (Western Anatolia, Turkey) by means of Bouguer gravity analysis. *Cumhuriyet Yerbilimleri Dergisi* 30: 71-86 (in Turkish with abstract in English).
- Ali MY, Fairhead JD, Green CM, Noufal A (2017). Basement structure of the United Arab Emirates derived from an analysis of regional gravity and aeromagnetic database. *Tectonophysics* 712-713: 503-522.
- Altinoğlu FF, Aydın A (2015). Interpretation of deep crust structure and linear features of western Anatolia by using Bouguer gravity data. *Proceedings of Azerbaijan National Academy of Sciences, Sciences of Earth* 3: 46-53.
- Altinoğlu FF, Sari M, Aydın A (2015). Detection of lineaments in Denizli basin of western Anatolia using Bouguer gravity data. *Pure Appl Geophys* 172: 415-425.
- Alvandi A, Babaei M (2017). Edge detection of gravity anomalies with directional hyperbolic tilt angles: application to synthetic and field data. *J Ind Geophys Union* 21: 13-16.
- Alvandi A, Rasoul H (2014). Edge detection process of Qom salt dome gravity anomalies using hyperbolic tilt angle. *International Journal of Geomatics and Geosciences* 5: 209-224.
- Ardestani VE (2005). Gravity interpretation via gravity gradients and analytic signal, *J Earth Sci* 12: 54.
- Ardestani VE, Motavalli H (2007). Constraints of analytic signal to determine the depth of gravity anomalies. *J Earth Space Phys* 33: 77-83.
- Arisoy MO, Dikmen U (2011). Potensoft: MATLAB-based software for potential field data processing, modeling and mapping. *Comput Geosci* 37: 935-942.
- Bayrak E, Yılmaz S, Bayrak Y (2017). Temporal and spatial variations of Gutenberg-Richter parameter and fractal dimension in Western Anatolia, Turkey. *J Asian Earth Sci* 138: 1-11.
- Bosum W, Damaske D, Roland NW, Behrendt J, Saltus R (1989). The Ganovex IV Victoria Land/Ross Sea aeromagnetic survey: interpretation of anomalies. *Geol Jahrb E* 38: 153-230.
- Bozkurt E, Sözbilir H (2004). Tectonic evolution of the Gediz Graben: field evidence for an episodic, two-stage extension in western Turkey. *Geol Mag* 141: 63-79.
- Bozkurt E, Sözbilir H (2006). Evolution of the large-scale active Manisa Fault, Southwest Turkey: implications on fault development and regional tectonics. *Geodin Acta* 19: 427-453.
- Chen G, Liu T, Sun J, Cheng Q, Sahoo B, Zhang Z, Zhang H (2015). Gravity method for investigating the geological structures associated with W-Sn polymetallic deposits in the Nanling Range. *China J Appl Geophys* 120: 14-25.
- Cheyney S, Hill I, Linford N (2011). Advantages to using the pseudogravity transformation to aid edge detection of total field archaeomagnetic datasets. *Archaeol Prosp* 18: 81-93.
- Çiğci G, Pamukçu O, Çoruh C, Çopur S, Sözbilir H (2011). Shallow and deep structure of a supradetachment basin based on geological, conventional deep seismic reflection sections and gravity data in the Büyük Menderes Graben, western Anatolia. *Surv Geophys* 32: 271-290.
- Çiftçi NB, Bozkurt E (2009). Structural evolution of the Gediz Graben, SW Turkey: temporal and spatial variation of the graben basin. *Basin Res* 22: 846-873.
- Cohen HA, Dart CJ, Akyuz HS, Barka A (1995). Syn-rift sedimentation and structural development of the Gediz and Büyük Menderes graben, western Turkey. *J Geol Soc London* 152: 629-638.
- Connard G, Couch R, Gemperle M (1983). Analysis of aeromagnetic measurements from the Cascade Range in central Oregon. *Geophysics* 48: 376-390.
- Cooper G, Cowan D (2004). Filtering using variable order vertical derivatives. *C R Geosci* 30: 455-459.
- Cooper GRJ, Cowan DR (2006). Enhancing potential field data using filters based on the local phase. *Comput Geosci* 32: 1585-1591.
- Cordell L (1979). Gravimetric expression of graben faulting in Santa Fe country and the Espanola Basin, New Mexico. In: *New Mexico Geological Society 30th Field Conference Guidebook*. Socorro, NM, USA: New Mexico Geological Society, pp. 59-64.
- Cordell L, Grauch VJS (1985). Mapping basement magnetization zones from aeromagnetic data in the San Juan Basin, New Mexico. In: Hinze, WJ, editor. *The Utility of Regional Gravity and Magnetic Anomaly Maps*. Tulsa, OK, USA: Society of Exploration Geophysicists, pp. 181-197.
- Çubuk-Sabuncu Y, Taymaz T, Fichtner A (2017). 3-D crustal velocity structure of western Turkey: constraints from full-waveform tomography. *Phys Earth Planet Inter*, 270: 90-112.
- Dewey JE, Şengör AMC (1979). Aegean and surrounding regions: complex and multiple continuum tectonics in a convergent zone. *Geol Soc Am Bull* 90: 84-92.
- Duman TY, Emre Ö (2011). 1:250,000 Scale Active Fault Map Series of Turkey, Aydın (NJ 35-11) Quadrangle. Serial Number: 7. Ankara, Turkey: General Directorate of Mineral Research and Exploration.
- Elmas A, Karşı H, Kadirov FA (2018). Lineaments in the Shamakhy-Gobustan and Absheron hydrocarbon containing areas using gravity data. *Acta Geophys* 66: 39-49.

- Emre Ö, Duman TY, Özalp S, Elmacı H (2011). 1:250,000 Scale Active Fault Map Series of Turkey, Denizli (NJ 35-12) Quadrangle. Serial Number: 12. Ankara, Turkey: General Directorate of Mineral Research and Exploration.
- Garcia-Abdeslem J, Ness GE (1994). Inversion of the power spectrum from magnetic anomalies. *Geophysics* 59: 391-401.
- Göktürkler G, Salk M, Sari C (2003). Numerical modeling of the conductive heat transfer in western Anatolia. *J. Balkan Geophy Soc* 6:1-15.
- Gómez-Ortiz D, Agarwal BNP (2005). 3DINVER.M: A MATLAB program to invert the gravity anomaly over a 3-D horizontal density interface by Parker-Oldenburg's algorithm. *Comput Geosci* 31: 513-520.
- Gout RE, Khattach D, Houari MR, Kaufmann O, Aqil H (2010). Main structural lineaments of north-eastern Morocco derived from gravity and aeromagnetic data. *J African Earth Sci* 58: 255-271.
- Guo LH, Meng XH, Zhang GL (2014). Three-dimensional correlation imaging for total amplitude magnetic anomaly and normalized source strength in the presence of strong remanent magnetization. *J Appl Geophys* 111: 121-128.
- Hahn A, Kind EG, Mishra DC (1976). Depth estimation of magnetic sources by means of Fourier amplitude spectra. *Geophys Prospect* 24: 287-308.
- Hornby P, Boschetti F, Horowitz FG (1999). Analysis of potential field data in the wavelet domain. *Geophys J Int* 137: 175-196.
- Işık M (1997). Değişken yoğunluklu sedimanter basen anomalilerinin ters çözümü. PhD, Kocaeli University, Kocaeli, Turkey.
- Işık M, Şenel H (2009). 3D gravity modeling of Büyük Menderes basin in western Anatolia using parabolic density function. *J Asian Earth Sci* 34: 317.
- Koçyiğit A, Yusufoglu H, Bozkurt E (1999). Evidence from the Gediz graben for episodic two-stage extension in western Turkey. *J Geol Soc London* 156: 605-616.
- Kumar NJ, Singh AP, Rao MRKP, Chandrasekhar DW, Singh B (2009). Gravity signatures derived crustal structure and tectonics of Achankovil shear zone Southern India. *Gondwana Res* 16: 45-55.
- Le Pichon X, Angelier J (1979). The Hellenic arc and trench system: A key to the neotectonic evolution of the eastern Mediterranean area. *Tectonophysics* 60: 1-42.
- Lyngsie SB, Thybo H, Rasmussen TM (2006). Regional geological and tectonic structures of the North Sea area from potential field modelling. *Tectonophysics* 413: 147-170.
- Ma G, Li L (2012). Edge detection in potential fields with the normalized total horizontal derivative. *Comput Geosci* 41: 83-87.
- McKenzie DP (1972). Active tectonics of the Mediterranean Region. *Geophys J Roy Astron Soc* 30: 109-185.
- Mickus K (2008). Regional gravity analysis of Burkina Faso: Implications for the location of metallic ore deposits. *J African Earth Sci* 50: 55-66.
- Miller HG, Singh V (1994). Potential field tilt -a new concept for location of potential field sources. *J Appl Geophys* 32: 213-217.
- Nabighian MN (1972). The analytic signal of two dimensional magnetic bodies with polygonal cross section: its properties and use for automated anomaly interpretation. *Geophysics* 37: 507-517.
- Nabighian MN, Ander ME, Grauch VJS, Hansen RO, Lafehr TR, Li Y, Pearson WC, Peirce JW, Phillips JD, Ruder ME (2005). Historical development of the gravity method in exploration. *Geophysics* 70: 63-89.
- Naouali BS, Inoubli MH, Amiri A, Chaqui A, Hamdi I (2011). Subsurface geology of the Ariana region (Diapir Zone, northern Tunisia) by means of gravity analysis. *Geophy Prosp* 59: 983-997.
- Nishijima J, Naritomi K (2015). Interpretation of gravity data to delineate underground structure in the Beppu geothermal field, central Kyushu, Japan. *J Hydrology Reg Stud* 11: 84-95.
- Oldenburg DW (1974). The inversion and interpretation of gravity anomalies. *Geophysics* 39: 526-536.
- Oruç B (2010). Edge detection and depth estimation using a tilt angle map from gravity gradient data of the Kozaklı-Central Anatolia Region, Turkey. *Pure Appl Geophys* 168: 1769-1780.
- Özelçi F (1973). Gravity anomalies of the Eastern Mediterranean. *Bulletin of the Mineral Research and Exploration* 80: 54-92.
- Pamukçu O, Yurdakul A (2008). Isostatic compensation in western Anatolia with estimate of the effective elastic thickness. *Turk J Earth Sci* 17: 545-557.
- Parker RL (1972). The rapid calculation of potential anomalies. *Geophys J R Astr Soc* 31: 447-455.
- Phillips JD (2000). Locating magnetic contacts; a comparison of the horizontal gradient, analytic signal, and local wavenumber methods. *Society of Exploration Geophysicists Abstracts with Programs* 402-405.
- Rabinowitz PD, Ryan WBF (1970). Gravity anomalies and crustal shortening in the Eastern Mediterranean. *Tectonophysics* 10: 285-608.
- Rapolla A, Cella F, Fedi M, Florio G (2002). Improved techniques in data analysis and interpretation of potential fields: examples of application in volcanic and seismically active areas. *Ann Geophys* 45: 6.
- Roest WR, Verhoef J, Pilkington M (1992). Magnetic interpretation using the 3D analytic signal. *Geophysics* 57: 116-125.
- Saibi H, Nishijima J, Ehara S (2006). Processing and interpretation of gravity data for the Shimabara Peninsula area, Southwestern Japan. *Mem Fac Eng Kyushu Uni* 66: 2.
- Sarı C, Şalk M (2002). Analysis of gravity anomalies with hyperbolic density contrast: An application to the gravity data of western Anatolia. *J Balkan Geophys Soc* 5: 87-96.
- Sarı C, Şalk M (2006). Sediment thicknesses of the western Anatolia graben structures determined by 2D and 3D analysis using gravity data. *J Asian Earth Sci* 26: 39-48.

- Şenel H (1997). Inversion of gravity anomaly of Büyük Menderes faults. *Journal of Kocaeli University* 4: 66-72 (in Turkish with abstract in English).
- Şengör AMC, Görür N, Şaroğlu F (1985). Strike-slip faulting and related basin formation in zones of tectonic escape: Turkey as a case study. *Soc Econ Paleontol Min Spec Pub* 37: 227-264.
- Seyitoğlu G, Scott B (1996). The age of the Büyük Menderes graben (west Turkey) and its tectonic implications. *Geol Mag* 129: 239-242.
- Seyitoğlu G, Scott B, Rundle CC (1992). Timing of Cenozoic extensional tectonics in west Turkey. *J Geol Soc London* 149: 533-538.
- Sözbilir H (2001). Extensional tectonics and the geometry of related macroscopic structures: field evidence from the Gediz Detachment, Western Turkey. *Turk J Earth Sci* 10: 51-67.
- Spector A, Grant FS (1970). Statistical models for interpreting aeromagnetic data. *Geophysics* 35: 293-302.
- Uieda L, Barbosa VCF (2012). Robust 3D gravity gradient inversion by planting anomalous densities. *Geophysics* 77: 55-66.
- Verduzco B, Fairhead JD, Green CM, MacKenzie C (2004). New insights into magnetic derivatives for structural mapping. *Lead Edge* 23: 116-119.
- Wang J, Meng X, Li F (2017). New improvements for lineaments study of gravity data with improved Euler inversion and phase congruency of the field data. *J Appl Geophys* 136: 326-334.
- Wang J, Meng XH, Guo LH, Chen ZX, Li F (2014). A correlation-based approach for determining the threshold value of singular value decomposition filtering for potential field data denoising. *J Geophys Eng* 11: 055007-7.
- Wang J, Meng XH, Li F (2015). Improved curvature gravity gradient tensor with principal component analysis and its application in edge detection of gravity data. *J Appl Geophys* 118: 106-114.
- Wijns C, Perez C, Kowalczyk P (2005). Theta map edge detection in magnetic data. *Geophysics* 70: 39-43.
- Yılmaz Y, Genç SC, Gurer OF, Bozcu M, Yılmaz K, Karacık Z, Altunkaynak S, Elmas A (2000). When did the western Anatolian grabens begin to develop? *Geo Soc London Spec Publ* 173: 353-384.
- Zuo BX, Hu XY (2015). Edge detection of gravity field using eigenvalue analysis of gravity gradient tensor. *J Appl Geophys* 114: 263-270.